
Article:
Hobbs, M.J., Grainger, M.P., Zhu, C. et al. (2 more authors) (2018) Quantitative thermal imaging using single-pixel Si APD and MEMS mirror. Optics Express, 26 (3). pp. 3188-3198. ISSN 1094-4087

https://doi.org/10.1364/OE.26.003188

Research Article | Vol. 26, No. 3 | 5 Feb 2018 | OPTICS EXPRESS 3188
Optics EXPRESS

Quantitative thermal imaging using single-pixel Si APD and MEMS mirror

MATTHEW J. HOBBS, MATTHEW P. GRAINGER, CHENGXI ZHU, CHEE HING TAN, AND JONATHAN R. WILLMOTT*

Department of Electronic and Electrical Engineering, The University of Sheffield, Sheffield, S1 4DE, UK
**j.r.willmott@sheffield.ac.uk*

Abstract: Accurate quantitative temperature measurements are difficult to achieve using focal-plane array sensors. This is due to reflections inside the instrument and the difficulty of calibrating a matrix of pixels as identical radiation thermometers. Size-of-source effect (SSE), which is the dependence of an infrared temperature measurement on the area surrounding the target area, is a major contributor to this problem and cannot be reduced using glare stops. Measurements are affected by power received from outside the field-of-view (FOV), leading to increased measurement uncertainty. In this work, we present a micromechanical systems (MEMS) mirror based scanning thermal imaging camera with reduced measurement uncertainty compared to focal-plane array based systems. We demonstrate our flexible imaging approach using a Si avalanche photodiode (APD), which utilises high internal gain to enable the measurement of lower target temperatures with an effective wavelength of 1 µm and compare results with a Si photodiode. We compare measurements from our APD thermal imaging instrument against a commercial bolometer based focal-plane array camera. Our scanning approach results in a reduction in SSE related temperature error by 66 °C for the measurement of a spatially uniform 800 °C target when the target aperture diameter is increased from 10 to 20 mm. We also find that our APD instrument is capable of measuring target temperatures below 700 °C, over these near infrared wavelengths, with D* related measurement uncertainty of ± 0.5 °C.

OCIS codes: (040.1345) Avalanche photodiodes (APDs); (110.6820) Thermal imaging; (120.6780) Temperature.

References and links

1. J. Dixon, "Radiation thermometry," J. Phys. E Sci. Instrum. **21**(5), 425–436 (1988).
2. P. Saunders, *Radiation Thermometry: Fundamentals and Applications in the Petrochemical Industry* (SPIE Ppress, 2007).
3. H. W. Yoon and G. P. Eppeldauer, "Measurement of thermal radiation using regular glass optics and short-wave infrared detectors," Opt. Express **16**(2), 937–949 (2008).
4. J. Spannar, P. Wide, and B. Sohlberg, "A method for measuring strip temperature in the steel industry," IEEE Trans. Instrum. Meas. **51**(6), 1240–1245 (2002).
5. F. J. Rodriguez, F. J. Meca, J. A. Jimenez, and E. J. Bueno, "Monitoring and quality improvement of pharmaceutical glass container's manufacturing process," IEEE Trans. Instrum. Meas. **57**(3), 584–590 (2008).
6. A. Bendada, K. Cole, M. Lamontagne, and Y. Simard, "Infrared radiometry using a dielectric-silver-coated hollow glass waveguide for polymer processing," Infrared Phys. Technol. **45**(1), 59–68 (2004).
7. Q. He, Z. Su, Z. Xie, Z. Zhong, and Q. Yao, "A Novel Principle for Molten Steel Level Measurement in Tundish by Using Temperature Gradient," IEEE Trans. Instrum. Meas. **66**(7), 1809–1819 (2017).
8. R. Usamentiaga, J. Molleda, D. F. Garcia, J. C. Granda, and J. L. Rendueles, "Temperature measurement of molten pig iron with slag characterization and detection using infrared computer vision," IEEE Trans. Instrum. Meas. **61**(5), 1149–1159 (2012).
9. J. Envall, S. Mekhontsev, Y. Zong, and L. Hanssen, "Spatial scatter effects in the calibration of IR pyrometers and imagers," Int. J. Thermophys. **30**(1), 167–178 (2009).
10. G. Grgić and I. Pušnik, "Analysis of thermal imagers," Int. J. Thermophys. **32**(1–2), 237–247 (2011).
11. H. Budzier and G. Gerlach, "Calibration of uncooled thermal infrared cameras," J. Sens. Sens. Syst. **4**(1), 187–197 (2015).

#305917 https://doi.org/10.1364/OE.26.003188
Journal © 2018 Received 14 Sep 2017; revised 8 Dec 2017; accepted 20 Dec 2017; published 30 Jan 2018

Optics EXPRESS

12. M. F. Duarte, M. A. Davenport, D. Takhar, J. N. Laska, T. Sun, K. F. Kelly, and R. G. Baraniuk, "Single-pixel imaging via compressive sampling," IEEE Signal Process. Mag. **25**(2), 83–91 (2008).
13. M.-J. Sun, M. P. Edgar, D. B. Phillips, G. M. Gibson, and M. J. Padgett, "Improving the signal-to-noise ratio of single-pixel imaging using digital microscanning," Opt. Express **24**(10), 10476–10485 (2016).
14. R. Usamentiaga, D. F. Garcia, and J. Molleda, "Uncertainty analysis in spatial thermal measurements using infrared line scanners," IEEE Trans. Instrum. Meas. **57**(9), 2074–2082 (2008).
15. L. Li, V. Stankovic, L. Stankovic, L. Li, S. Cheng, and D. Uttamchandani, "Single pixel optical imaging using a scanning MEMS mirror," J. Micromech. Microeng. **21**(2), 025022 (2011).
16. W. Aenchbacher and T. Kurzweg, "Single-pixel, MEMS scanning mirror camera," in *IEEE Photonic Society 24th Annual Meeting* (IEEE, 2011), pp. 849–850.
17. R. Moss, P. Yuan, X. Bai, E. Quesada, R. Sudharsanan, B. L. Stann, J. F. Dammann, M. M. Giza, and W. B. Lawler, "Low-cost compact MEMS scanning LADAR system for robotic applications," Proc. SPIE **8379**, 837903 (2012).
18. V. Milanović, A. Kasturi, J. Yang, and F. Hu, "Closed-Loop Control of Gimbal-less MEMS Mirrors for Increased Bandwidth in LiDAR Applications," Proc. SPIE **10191**, 101910N (2017).
19. M. Hobbs, C. Tan, and J. Willmott, "Evaluation of phase sensitive detection method and Si avalanche photodiode for radiation thermometry," J. Instrum. **8**(3), P03016 (2013).
20. G. R. Peacock, "A review of non-contact process temperature measurements in steel manufacturing," Proc. SPIE **3700**, 171–189 (1999).
21. L. Chen, H. Gao, Y. Zhao, Y. Yu, and D. Wang, "Temperature error in casting radiation thermometry caused by emissivity error and measurement wavelength," in *ICIEA 2008: 3rd IEEE Conference on Industrial Electronics and Applications* (IEEE, 2008), pp. 1047–1049.
22. Hamamatsu Photonics, "Si photodiodes - S1087/S1133 series," http://www.hamamatsu.com/resources/pdf/ssd/s1087_etc_kspd1039e.pdf. Last Accessed: August, 2017.
23. Hamamatsu Photonics, "Si APD - S9251/S12092 series," http://www.hamamatsu.com/resources/pdf/ssd/s9251_etc_kapd1013e.pdf. Last Accessed: August, 2017.
24. J. Hahn and C. Rhee, "Interpolation equation for the calibration of infrared pyrometers," Metrologia **31**(1), 27–32 (1994).
25. J. Bezemer, "Spectral sensitivity corrections for optical standard pyrometers," Metrologia **10**(2), 47–52 (1974).
26. P. Saunders, "Uncertainty Arising from the Use of the Mean Effective Wavelength in Realizing ITS-90," in *AIP Conference Proceedings* (AIP, 2003), pp. 639–644.
27. A. Whittam, R. Simpson, and H. McEvoy, "Performance tests of thermal imaging systems to assess their suitability for quantitative temperature measurements," in *12th International Conference on Quantitative InfraRed Thermography* (QIRT, 2014).

1. Introduction

Radiation thermometers are commonly used to measure the temperature of target objects by measuring their emitted infrared radiation [1–3]. They can be used for industrial processing applications, for instance for various metals, glass and plastics during manufacture [4–6], where accurate temperature measurement is required for quality control and energy efficiency. The non-contact measurement nature of the radiation thermometer allows it to be easily moved to measure the temperature of different points on the target by re-sighting the instrument, with both fixed and portable instruments available. Compared to contact temperature measurements, it offers the added benefits of higher speed operation whilst eliminating the risk of contamination of the target object. Taking the non-contact measurement approach further, the use of infrared detector arrays within thermal imaging cameras allow for measurement over a wider area, enabling a temperature map to be produced without having to move the sighting position [7,8].

The use of thermal imaging cameras is particularly helpful for qualitative thermal imaging applications, although they are relatively expensive. For example, they can be used to detect spatial temperature variations across the target, which could indicate problems within the manufacturing process. However, thermal imaging cameras have disadvantages compared to quantitative radiation thermometry, when measurement of target temperature with low uncertainty is required. Quantitative thermal imaging allows SI unit traceable temperature measurements with defined or quantifiable uncertainty made on a grid across the camera scene. This is in contrast to thermal imaging cameras that provide qualitative temperature maps that can distinguish between different gradients of temperature. Under the precise methodology in which they were calibrated they will provide accurate temperature measurement; however away from those experimental conditions they provide only indicative

Optics EXPRESS

temperature measurements. A significant problem within thermal imaging cameras is the size-of-source effect (SSE), which arises due to imperfections within the optical system leading to reflections and scattering. Each pixel receives power over a wider area of the target than the camera was designed for [9,10]. Glare stops may reduce the problem, though this approach is far less effective than for single-pixel systems where all but the single-pixel surface can be made highly absorbing. With an array of pixels, the measured temperature becomes dependent upon the size of the target or objects next to the target. Thermal imaging cameras require more steps in the calibration process, with each individual pixel requiring calibration and unresponsive pixels being accounted for [11]. Other concerns include inter-pixel crosstalk and non-uniformities across the array, both in terms of within the semiconductor material, electronic noise or the ambient temperature. The price of focal-plane array based thermal imaging cameras increases dramatically as the operating wavelength, λ_{op}, increases (especially if cooling is required). Cheaper uncooled thermal detector based arrays can be used at longer wavelengths, at the expense of lower sensitivity and lower speed operation.

Single-pixel imaging has been explored for different applications using digital micromirror devices (DMDs) utilising compressive sampling algorithms [12,13]. Unfortunately, availability of window materials limits their operation to $\lambda_{op} < 2.5$ µm. An approach commonly used in industry is that of rotating mirror scanners which rapidly move the measurement FOV across the target in 1-dimension, and are particularly suited to moving targets, such as on a conveyor belt or for metal strips being rolled [14]. They offer advantages over conventional focal-plane array based imaging cameras: reduced SSE, simplified calibration and reduced cost for longer wavelength operation. A new approach to mirror scanning in recent years is the use of microelectromechanical systems (MEMS) mirror based imaging, which has been previously demonstrated using visible light [15,16] and LiDAR [17,18]. Such mirrors offer high speed 2-dimensional beam steering by devices which can be fabricated using low cost Si wafers.

Limitations in technology constrains MEMS mirrors to be comparatively small; typically only a few millimetres in diameter. The power reaching the detector within a MEMS based scanning system is, in turn, limited by the small size of currently available mirrors. This vignettes the optical system or leads to a slow optical system with a large f-number, therefore, limiting the lowest temperature which can be measured by the instrument. High resolution imaging (for both scanned imagers and focal-plane array imagers), requires small active area detectors or pixels. However, use of smaller area detectors leads to comparatively reduced irradiance at the detector surface, also limiting the lowest temperature which can be measured by the instrument with acceptable signal-to-noise-ratio (SNR). We have previously demonstrated a Si avalanche photodiode (APD) as an alternative detector to a Si photodiode for radiation thermometry operating at $\lambda_{op} = 1$ µm, successfully demonstrating that the high internal gain of the APD allows lower target temperatures to be measured [19]. Therefore a Si APD would appear to be an ideal candidate for single-pixel thermal imaging with $\lambda_{op} = 1$ µm. Radiation thermometry with $\lambda_{op} = 1$ µm is commonly used for general purpose high temperature (> 600 °C) applications such as in the steel industry [20], where its spectral response is within the range of the corresponding blackbody spectra at such temperatures. Operating at this short wavelength also has the advantage that it will result in reduced error in the measured temperature caused by unknown target emissivity compared to longer wavelength operation [21].

In this work, we present a 1 µm MEMS mirror based single-pixel thermal imaging camera for quantitative thermal imaging, comparing both a Si APD and a Si photodiode as the chosen sensor. The comparison enables a demonstration of the benefits provided by a Si APD for single-pixel thermal imaging over a Si photodiode. To further demonstrate the benefits of this imaging approach for quantitative thermal imaging, comparison is also made with a commercial bolometer based focal-plane array imager. Our scanning approach results in a reduction in SSE related temperature error by 66 °C for the measurement of a spatially

Optics EXPRESS

uniform 800 °C target when the target aperture diameter is increased from 10 to 20 mm. Our instrument is capable of measuring a target temperature below 700 °C with a noise performance of better than ± 0.5 °C. To the best of our knowledge, this is the first use of a Si APD (or any APD) for thermal imaging for quantitative temperature measurement.

2. Experimental design and procedures

The experimental setup for the MEMS single-pixel thermal imaging camera is shown in Fig. 1.

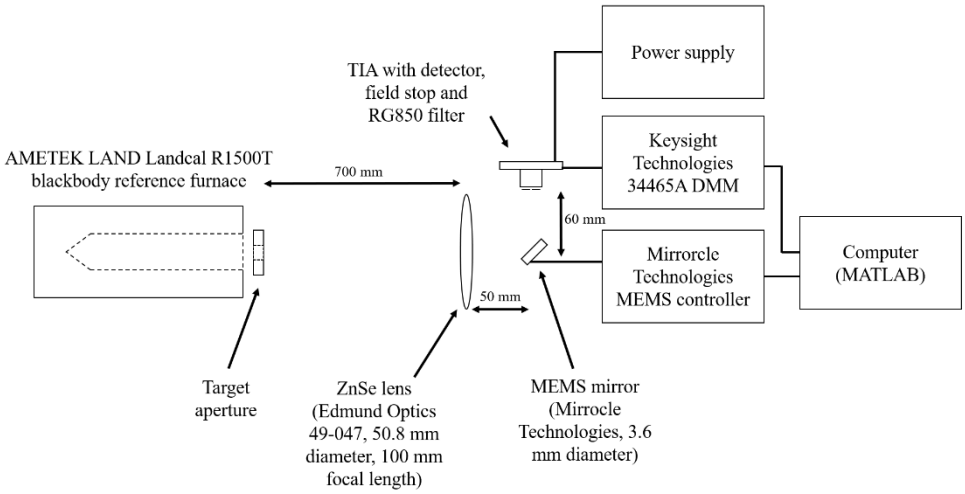

Fig. 1. MEMS single-pixel thermal imaging setup diagram.

The instrument generates a bidirectional raster scanning pattern of the single-pixel's FOV. The FOV is scanned across 320 horizontal positions and 78 vertical positions with the signal measured by the detector at each scan position or 'pixel'. The signal is amplified by a transimpedance amplifier (TIA) and logged by a MATLAB controlled digital multimeter (DMM). In this work, we compared a Si photodiode and a Si APD, using Hamamatsu S1133-01 and Hamamatsu S12092-2, respectively [22,23]. The TIA circuit was of conventional configuration, and comprised a Texas Instruments OPA657 op-amp and a resistor-capacitor (RC) feedback network (2 MΩ and 1.8 pF), giving a circuit rise time of ~8 µs. The TIA circuit was followed by a first order RC filter (1 kΩ and 1 nF) for additional noise rejection. In order to supply a constant high voltage to the APD, a Laser Components ABC550-06 biasing module was used. For data capture, the voltage measurement for each pixel takes approximately 4.4 ms (of which 4 ms is the integration time of the DMM); this is significantly slower than the TIA circuit response time. The full image can be captured within approximately 110 seconds; with the MEMS mirror positions pre-loaded and stored locally within the flash memory of the MEMS controller to avoid adding additional time to the image capture. This slow acquisition time could be improved by implementing a faster method of analogue-to-digital conversion.

A 0.2 mm field stop was located in front of the Si photodiode to enable resolution and power throughput measurements to be compared with the 0.2 mm diameter active area of the APD. Under these conditions, the FOV of the single-pixel was found to be approximately 5 mm in diameter for both the Si photodiode and Si APD imagers. An RG850 daylight filter was placed in front of each detector, to reduce the effect of background light on the measurement and to define the short wavelength spectral response of the detectors.

Optics EXPRESS

Planck's law can be used to mathematically model the radiant exitance from a blackbody as a function of wavelength and temperature. At wavelengths that are short compared to the peak in emission, an approximation that can be algebraically manipulated is given by the Wien law, as shown in (1).

$$L(\lambda) = \frac{c_1}{\lambda^5} \exp\left(\frac{-c_2}{\lambda T}\right) \tag{1}$$

L is the spectral radiance of the emitted radiation of an ideal blackbody, c_1 is Planck's first radiation constant, c_2 is Planck's second radiation constant, λ is wavelength and T is the blackbody temperature in kelvin. From (1), the relationship between the measured output voltage, V, and the target temperature can be approximated by plotting $\ln(V)$ against $1/T$ [24]; V is proportional to L. The gradient of this plot enables us to calculate a useful approximation of the mean effective wavelength for the instrument, λ_m, which is an average wavelength of the detector spectral response over the measured temperature range [25,26]. Ideally, the $\ln(V)$ against $1/T$ relationship would be linear in radiance and would allow a simple calibration at a single point in the instrument temperature measurement range. A non-linear response is also usable, when used with multiple calibration temperatures and a more involved calibration procedure. Si photodiodes are highly linear, which makes them ideal for calibration, whereas Si APDs as a function of radiance may be non-linear and will be a subject of our analysis.

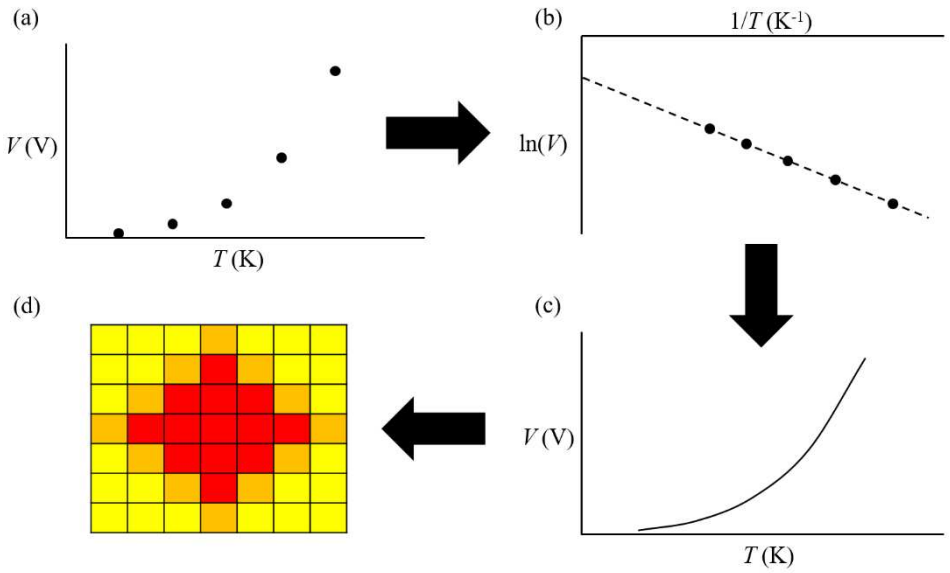

Fig. 2. Single-pixel imager calibration steps.

The basic calibration procedure for the single-pixel thermal camera is shown in Fig. 2. The output voltage as a function of furnace temperature was measured, with the dark offset voltage first measured and subtracted from each point, (a). A 10 mm target aperture was used for calibration in this work, which was approximately twice the diameter of the FOV of the single-pixel. The factor of two accounts for the design FOV and, in addition, any radiation from outside the FOV due to the SSE. The $\ln(V)$ against $1/T$ relationship was plotted, (b), and the gradient, m, and intercept, c, were found and used in the calibration equation, Eq. (2).

$$V = \exp\left(\frac{1}{T}m + c\right) \tag{2}$$

Optics EXPRESS

This calibration equation was used to calculate the output voltage expected for different target temperatures, or conversely the temperature each measured voltage corresponds to, (c). This calibration can therefore be applied to the thermal image to produce a temperature map showing how the measured temperature varies across the image, (d).

The D* related temperature noise was estimated by extracting the mean and standard deviation of the temperature measurement data with the MEMS mirror stationary at its origin position whilst imaging a 10 mm target aperture. The root-mean-squared (RMS) noise of the instrument was calculated by taking 2 × the standard deviation value, which therefore represents the fluctuation in the measured temperature within ± 1 standard deviation from its mean.

3. Results and discussion

The assessment of our scanning thermal imaging camera was limited to those parameters most salient to quantitative radiation thermometry: SSE, noise and measurement uncertainty. This is sufficient because we are free from the usual problems of focal-plane array based thermal imaging.

In order to use an APD within any optical system, the optimum biasing voltage should first be evaluated for the circuit and application. Increased APD gain will provide benefit to the system up to a point where the excess noise generated by the APD becomes larger than the noise of the TIA. For our APD-TIA circuit, a biasing voltage of approximately −220 to −225 V was found to achieve peak SNR. We have not attempted to accurately quantify the level of internal gain for the APD; this requires knowledge of the APD's field profile to establish a unity gain reference [19]. However, with reference to the datasheet, the gain at this bias voltage should be greater than 2 orders of magnitude [23]. Note, this bias value for the APD is approximate, it is adjusted by the temperature compensation of the biasing module in order to keep the gain constant to overcome ambient temperature drift. For the Si photodiode, without internal gain, an operating bias of 0 V was used to minimise dark current.

The mean output voltage is shown in Fig. 3(a) as a function of furnace temperature for both the Si photodiode and Si APD. The output voltage of the Si APD camera is significantly higher across the measurement range (by over 2 orders of magnitude) compared to the Si photodiode based instrument. This is due to the high internal gain of the APD, which provides electronic gain to the output voltage measured, by increasing the photocurrent, without concomitant increase in noise seen in other methods of providing amplification. The APD can, therefore, be used to measure lower target temperature before the noise floor is reached. For instance, if a minimum output voltage of 1 mV is specified, the APD circuit produced this at a target temperature of ~584 °C, which is ~328 °C lower than the photodiode's minimum temperature of ~912 °C.

From Fig. 3(a) the APD output was found to obey Eq. (2) and hence is linear for measured temperatures down to 700 °C. At lower temperatures, non-linearity was observed. The non-linearity is not due to the total optical power, as the power is weak at all measured target temperatures. However, when the temperature reduces, the profile of photons from different wavelength changes. Since avalanche gain is also dependent on carrier injection profile, the gain therefore changes with the photon injection profile leading to a non-linear response. Our results are valid over the measured target temperature range due to the calibration process.

Optics EXPRESS

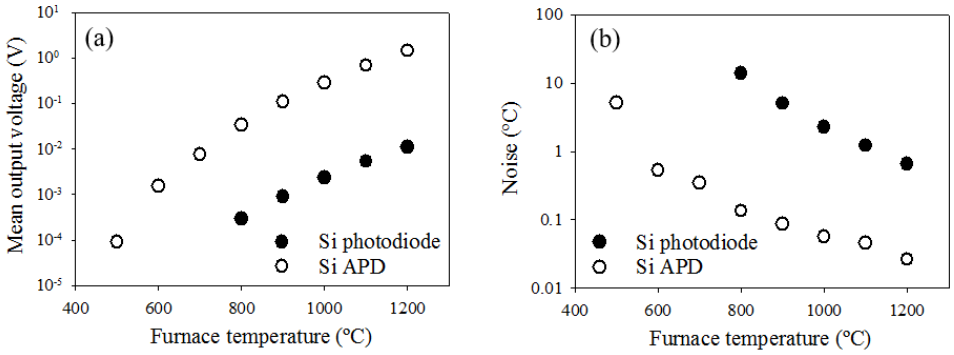

Fig. 3. (a) Mean output voltage and (b) noise for Si photodiode and Si APD imagers with furnace temperature.

Figure 3(b) shows the noise as a function of target temperature for both the Si photodiode and Si APD imagers. D* related noise dictates the minimum temperature that can be resolved for a temperature fluctuation and can be expressed as a temperature measurement uncertainty in degrees Celsius (e.g., within ± 0.5 °C of the measured temperature, which is a typical specification for a high quality radiation thermometer). Therefore, if the target signal measured is too weak, a reliable measure of the target temperature will not be possible. The noise of the Si APD is significantly less than that of the Si photodiode. If a ± 0.5 °C noise specification is required for the instrument, this would not be achieved by the Si photodiode over the measured temperature range. However, the Si APD would achieve the ± 0.5 °C noise specification for target temperatures of approximately 700 °C and above. The improved noise performance of the Si APD instrument is due to two reasons; the high internal gain of the APD, and its low junction capacitance compared to the Si photodiode. Circuit noise analysis calculations produced a total integrated circuit noise of 48 µV for the Si APD, and 880 µV for the Si photodiode; an improvement factor of over 18. The high capacitance of the large area Si photodiode led to increased gain at high frequencies, resulting in its increased noise. However, the factor of improvement in the noise measurement across all temperatures is greater than 18, and significantly better as the target temperature decreases. Therefore, even if the capacitance of the Si photodiode were to be the same as that of the APD, significant improvement would still be expected due to the high gain of the APD, especially at lower target temperatures. The improved noise and mean output voltage performance highlight both the advantage of, and requirement for, the Si APD in such an aperture limited system; the Si photodiode performance without high internal gain would not be sufficient.

Optics EXPRESS

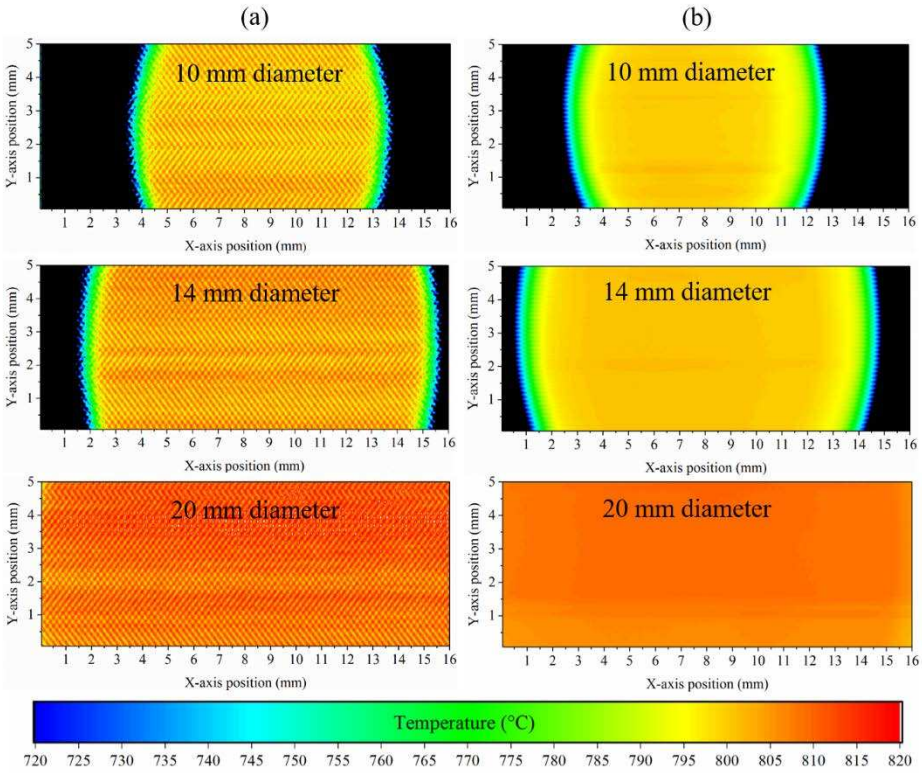

Fig. 4. SSE analysis for (a) Si photodiode and (b) Si APD imagers with increasing target aperture size at a furnace temperature of 800 °C.

Fully calibrated thermal imaging measurements are shown in Fig. 4 at a furnace temperature of 800 °C for both the Si photodiode and Si APD imagers. The imaged target aperture was increased in size to perform an SSE analysis; the raw data was calibrated at the 10 mm target aperture to provide a quantitative temperature measurement assessment. The imaged area is approximately 16 mm by 5 mm. By closely examining the images in Fig. 4, the imaged apertures do indeed correspond to the size of the target apertures used, hence demonstrating that the proof-of-concept works. Regards the temperature measurement within the image, there is a clear distinction between the Si photodiode and Si APD results. The Si APD's image is relatively uniform in temperature, whilst the Si photodiode's image shows a larger temperature variation. This is due to the much higher noise of the Si photodiode producing such a large fluctuation in temperature. To demonstrate the effect of this noise more clearly, cross sections were taken at the mid-points of the thermal images for the 10 mm target aperture, as shown in Fig. 5. The fluctuation in the measured temperature is clearly much less for the Si APD imager, which corresponds to its lower noise. These results highlight the importance of noise within a radiation thermometry / thermal imaging system and the benefit the Si APD provides due to its high internal gain leading to improved SNR performance.

Optics EXPRESS

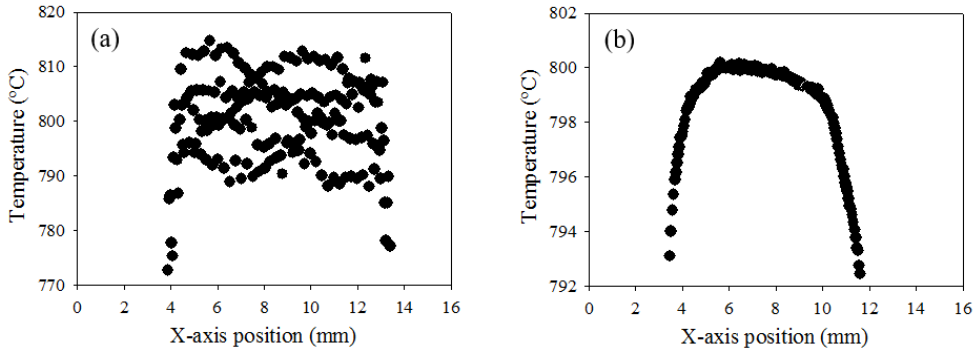

Fig. 5. Mid-point cross sections of the 10 mm target aperture thermal images for (a) Si photodiode and (b) Si APD imagers at a furnace temperature of 800 °C.

Moving from the centre to the periphery of each aperture for each of the two systems, Fig. 4 shows there is a reduction in the measured temperature and some blurring in the image at its very edges. This is believed to be due to the translation of the target spot over the aperture edge, where the FOV is elongated due to the finite response time of the detection electronics. As the target aperture size increases for both imagers, so does the measured temperature. This is believed to be due to residual SSE within the instrument, and is particularly clear as we increase the size of the target aperture. For the 20 mm target aperture, we measured approximately 10 °C increase in measured temperature compared with the 10 mm target aperture, which corresponds to 0.1% of the imager's dynamic range.

The primary motivation behind this work is to improve the accuracy of quantitative thermal imaging compared to what is currently possible with conventional focal-plane array thermal imaging. Issues with thermal imaging cameras for quantitative thermal imaging, primarily due to SSE issues, are well known but not well publicised. Unfortunately, this leads to thermal imaging cameras being used for quantitative temperature measurement applications without an understanding of their limitation in providing accuracy. For instance, a thermal detector based thermal imager could be used as a 'general purpose' method for measuring temperature without consideration of SSE, therefore resulting in a temperature error which is often ignored by the user. In order for us to make a direct comparison with a commercial thermal imaging camera, we repeated the imaging measurements with a bolometer based thermal imaging camera. The camera was focused onto the same target apertures as before. The approximate blackbody calibration furnace was set to 800 °C, and the images were cropped to show the same target area as our single-pixel camera. Results are shown in Fig. 6, with increasing target aperture size. The Si APD single-pixel camera was compared and temperature calibration was again relative to the 10 mm target aperture; cross sections of all the image mid-points are shown in Fig. 7. Although the imaging data for the bolometer camera provides faithful spatial information of the size of the target apertures, there is a large difference in the measured temperature when moving from the centre to the periphery, as is highlighted by examining the cross sections. Although this is the case, to some extent, for the Si APD single-pixel camera, it is a marked improvement over the bolometer camera. This SSE problem with the focal-plane array is particularly striking as the target aperture is increased in size. For the 20 mm aperture, the measured temperature is 876 °C, therefore an error of 76 °C compared to the 10 mm target aperture, corresponding to 3.5% of its dynamic range. This is considerably more than that of the Si APD single-pixel change of 10 °C. These results highlight the problem of SSE within staring array imagers for quantitative temperature measurement, and the benefits of our single-pixel imaging approach using a Si APD. When the target aperture diameter is increased from 10 to 20 mm, our single pixel thermal camera offers 66 °C improvement in SSE related temperature error for the

Optics EXPRESS

measurement of the 800 °C target. Our findings reflect the general understanding of this issue that has also be highlighted in investigations made by others [27].

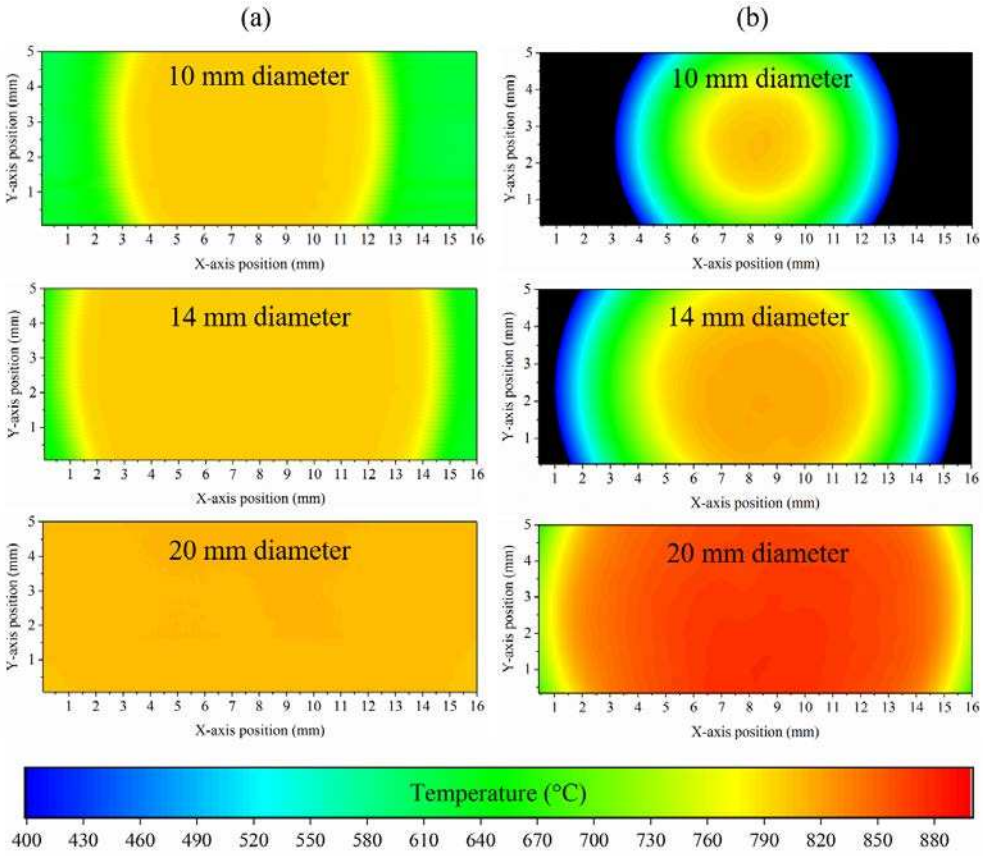

Fig. 6. SSE analysis for (a) Si APD and (b) bolometer camera imagers with increasing target aperture size at a furnace temperature of 800 °C.

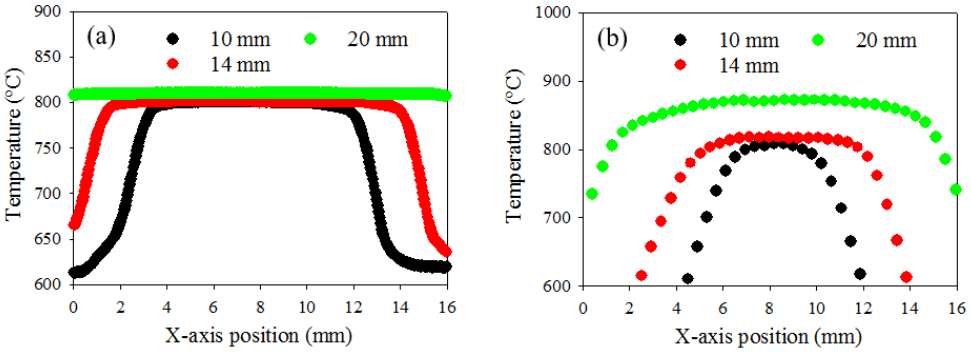

Fig. 7. Mid-point cross sections of the thermal images for (a) Si APD and (b) bolometer camera imagers at a furnace temperature of 800 °C.

With further investigation into causes of SSE within our Si APD thermal imager, we would expect to improve the performance even further. Primarily, causes of reflections should

Optics EXPRESS

be identified and greatly reduced. Suitable methods would be to fully enclose the setup, incorporate appropriate stops and baffles and to apply anti-reflection coating to the lens and MEMS mirror window.

4. Conclusion

In this work we have demonstrated a single-pixel MEMS based thermal imaging camera for quantitative temperature mapping. Both a Si photodiode and a Si APD were assessed and compared for the application. The high internal gain of the Si APD was shown to have a clear advantage over the Si photodiode, allowing for a lower temperature target to be imaged with a much lower noise quantitative temperature measurement. The Si APD single-pixel thermal imaging camera measures a target temperature of 700 °C with a noise performance better than ± 0.5 °C. In comparison with a commercial focal-plane array bolometer based camera, the greatly reduced SSE of our Si APD imager led to significant reduction in temperature error within the quantitative temperature measurement. For a target temperature of 800 °C, our single-pixel imager was shown to offer a 66 °C improvement in the SSE related temperature error when increasing the target aperture diameter from 10 to 20 mm. With further investigations and optimisation of the SSE within the Si APD imager, we would expect to reduce the measurement uncertainties further.

Funding

Engineering and Physical Sciences Research Council (EPSRC) fellowship EP/M009106/1.